Available online at www.sciencedirect.com
SCIENCE DIRECT®
Journal of Sound and Vibration 282 (2005) 1273–1284
JOURNAL OF SOUND AND VIBRATION
www.elsevier.com/locate/jsvi

Short Communication

Noise and vibration analysis of a disc–brake system using a stick–slip friction model involving coupling stiffness

Manish Paliwal[a,*], Ajay Mahajan[b], Jarlen Don[b], Tsuchin Chu[b], Peter Filip[c]

[a]*Department of Surgery/Orthopaedics, Southern Illinois University School of Medicine, Springfield, IL 62794-9672, USA*
[b]*Department of Mechanical Engineering and Energy Processes, Southern Illinois University at Carbondale, Carbondale, IL 62901, USA*
[c]*Center for Advanced Friction Studies, Southern Illinois University at Carbondale, IL 62901-4343, USA*

Received 29 April 2003; accepted 7 May 2004

1. Introduction

Brake-induced noise and vibration are serious concerns in the automotive industry due to the annoyance to the consumer. The most common noise is squeal and is defined as noise whose frequency content is 1000 Hz or higher that leads to excessively high and irritating sound pressure levels [1]. Resonance or high amplitudes results due to a frequency match in linear systems, while resonance in nonlinear system may occur at excitation frequencies that are not equal to the linear system's natural frequency [2]. Even a harmonic excitation provided by the stick–slip phenomenon may turn the system into a non-periodic or chaotic motion. Non-linearity provided by the stick–slip phenomenon includes not only variation in the coefficient of friction but also the variation in contact stiffness due to formation of friction layers on the interface [3]. It is hypothesized that this significant variation in layer stiffness modifies the behavior of the system. Formulation of a brake pad is very complex, with 10–30 components in the matrix [4]. A control in the bulk properties of a brake pad in terms of stiffness, damping and friction properties may help to avoid such behavior in the system. This is largely categorized into two theories, viz., stick–slip phenomenon and the vibrations resulting from the geometric instabilities of the brake

*Corresponding author. Tel.: +1-217-545-7303.
E-mail address: mpaliwal@siumed.edu (M. Paliwal).

0022-460X/$ - see front matter
doi:10.1016/j.jsv.2004.05.005

assembly [5]. Squeal has been categorized as low- and high-frequency squeals for the purpose of analysis [6]. The frequency ranges for the low-frequency squeal is 1000–2600 Hz and for high-frequency squeal is 2–15 kHz.

The squeal is affected by the pad, rotor and brake assembly material and geometry [7]. It not only depends on the bulk properties of the contact surfaces but also on the surface properties. The physical–chemical properties of the contact surface and the nonlinear variation of coefficient of friction due to the variation in temperature, velocity, pressure and environmental conditions affect its occurrence [3,4,8–12]. Sprag–slip effect of the shoe against the rotor has also been reported as one probable cause of squeal [13]. Geometrically induced instability or kinematic instability also emphasizes the physical parameters of the system along with the coefficient of friction as a reason for squeal [14]. System instabilities are generated due to changes in the direction of both normal and frictional forces (binary flutter theory) and are based on the dynamic characteristics of the rotor [15]. Squeal is also attributed to the complex modes of vibration which are interpreted as traveling waves [16]. This phenomenon was also experimentally verified [17]. Another study of power flow between interactive components concluded that the coupling between in-plane and transverse displacements of the rotor generates dynamic instabilities and brake squeal [18]. A critical review of research in brake noise and vibration is given by Ioannidis et al. [19].

The friction materials are abrasive and adhesive and interfacial reactions take place between the rubbing surfaces. Due to asperities between the rubbing surfaces, there is a formation of many micro-contact points which keep on changing dynamically in fraction of seconds during rubbing [18]. The contact area increases with the use of the softer brake-lining materials thereby decreasing the temperature of the friction surface. Temperature of the contact points may exceed the temperature of the solid–liquid line of the iron carbon binary system [18]. In automotive brakes, temperatures as high as 1000 °C were reported on the friction surface [3]. Atomic scale theory is also given for this phenomenon [10]. The crystal lattices of both solid materials, which are in contact, deform elastically when shear stress is applied on them. If more shear stress is applied, atoms come back to their new positions of equilibrium via plastic deformation. The crystal lattice vibrates until all the elastic energy is dissipated in the form of heat.

During a typical brake engagement friction coefficient starts rising initially and the temperature also increases with development of better contact. During this period, the flash temperature at the asperities may reach 1100 °C, within 1 ms and then cool down when other asperities also become active [3,20]. High temperature and friction coefficients facilitate intense material transfer. With the formation of the transfer layer and a decrease in its surface roughness and wear, the temperature and coefficient of friction stabilize [21]. Initially, there is major material transfer from the brake-lining pads on the cast iron rotor surface. But with time, as the temperature rises, there is plastic deformation of the cast iron surface layer, which may destroy its virgin pearlitic cast iron microstructure [22]. The composition and the characteristics of the surface layer are a function of the bulk formulation, temperature, pressure and relative velocity of the pad and rotor. Surface roughness and the differences in mechanical properties of the different constituents also play a significant role. The transfer layer's growth and thickness is dependent on the bulk material. Sometimes it is homogenous or it can be in the form of small island-like deposits [21]. The growth of friction layers affects the contact stiffness considerably, thereby affecting stability of the system. In friction-induced vibration, the excitation is derived from stick–slip and asperity junctions

engage and disengage during continuous sliding [23]. Hence, consideration of the interface properties becomes important for the study of the system.

The composition and the characteristics of the surface layer are a function of the bulk formulation, temperature, pressure and relative velocity of the pad and rotor. Surface roughness and the differences in mechanical properties of the different constituents also play a significant role. The transfer layer's growth and thickness is dependent on the bulk material. Sometimes it is homogenous or it can be in the form of small island-like deposits [21]. The growth of friction layers affects the contact stiffness considerably, thereby affecting stability of the system. In friction-induced vibration, the excitation is derived from stick–slip and asperity junctions engage and disengage during continuous sliding [23]. Hence, consideration of the interface properties becomes important for the study of the system.

In this work, the model presented by Shin et al. [24] is extended with the incorporation of the layer stiffness due to the formation of friction layers on the contact surface. Parametric studies have been carried out and the effect of the variation in layer stiffness on the system stability has been studied and conclusions drawn.

2. The 2-degree-of-freedom (DOF) disc–pad model

The model presented in Fig. 1 is considered in this study. The pad and rotor disc are modeled as single-degree-of-freedom systems which are connected through a sliding friction interface and interfacial coupling stiffness. Here m, k and c are the mass, stiffness and damping coefficients, respectively. System with subscript '1' refers to the pad, subscript '2' refers to the disc system, and the subscript '3' refers to the interfacial (friction layer) coupling system. The stiffness of the brake pad overlapped with the shear stiffness of the friction layer would be the stiffness at the interface. In the study k_3 is the coupling stiffness which is equivalent to the stiffness of the brake pad and friction layer in parallel. Friction layers and triboparticulates govern the interfacial properties [3,23]. Here, the term ''coupling stiffness'' represents the effective coupling stiffness between the brake pad and the rotor. The coupling stiffness between the rotor and the pad is composed of two parts: (1) the stiffness due to the friction layer on the rotor and the pad. (2) The modal stiffness of the pad at the coupling mode; the coupling of the modes occurs when they are close to each other.

Coupling stiffness = Layer stiffness + Modal stiffness of the pad at the coupling mode. Hence, the coupling stiffness (k_3) is determined by considering the layer stiffness (k_l) and the modal

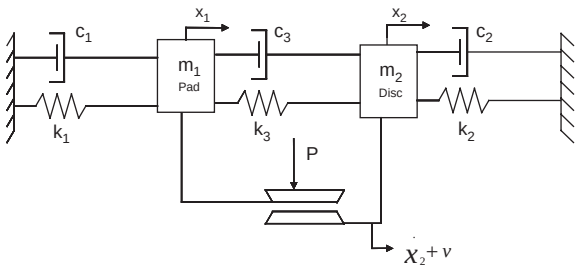

Fig. 1. Modeling the friction-induced vibration in a 2-dof system.

stiffness of the pad (k_{mp}) in series:

$$\frac{1}{k_3} = \frac{1}{k_{mp}} + \frac{1}{k_l}. \tag{1}$$

Here, k_{mp} is the modal stiffness of the pad and k_l is the layer stiffness.

Modal frequencies and modal stiffness of the pad can be determined and used for the in-plane model as in-plane modes exist at frequencies comparable to those for out-of-plane bending even for thickness to diameter ratio as small as 0.1 [25].

N is the normal force acting on the interface, where $N = P \cdot A$. The pressure (P) is applied on the interface and A is the surface area of contact. It is assumed that the applied force is constant initially, in spite of the fact that it varies in real-time applications. Hence, the growth in contact surface is considered to be a function of time. The contact becomes stable and constant at infinite time. The contact surface area also involves the evolution of friction layers which significantly influence system stiffness and friction characteristics of the contact. This effect of variation in coupling stiffness has been studied to appreciate the system stability using phase space diagrams. The size of the limit cycle gives an indication of the degree of severity of a noisy condition. A limit cycle is an attracting set to which orbits or trajectories converge and upon which trajectories are periodic.

Relative velocity is defined as

$$v_{\text{rel}} = \dot{x}_2 - \dot{x}_1 - v, \tag{2}$$

where v is the imposed velocity. If absolute relative velocity between pad and disc is less than or equal to η ($\eta \ll v$), the motion is considered in stick phase and in slip phase when $v_{\text{rel}} > \eta$.

$$F_{f_s} = k_1 x_1 + c_1 x_1 - k_2 x_2 - 2k_3(x_2 - x_1) - 2c_3(\dot{x}_2 - \dot{x}_1). \tag{3}$$

In deriving Eq. (3), the static force proposed by Shin et al. [24] has been used and extrapolated to make it applicable to the model at hand.

Equations of motion are given by

$$m_1\ddot{x}_1 + c_1\dot{x}_1 + k_1 x_1 - k_3(x_2 - x_1) - c_3(\dot{x}_2 - \dot{x}_1) = f, \tag{4}$$

$$m_2\ddot{x}_2 + c_2\dot{x}_2 + k_2 x_2 + k_3(x_2 - x_1) + c_3(\dot{x}_2 - \dot{x}_1) = f. \tag{5}$$

Here, effective friction force f is defined as

$$f = f_{v_{\text{rel}}} - f(v). \tag{6}$$

Here $f(v) = N(\mu_s - \alpha v)$, which is an offset compensation parameter; α is the slope of friction-velocity curve (Fig. 2). The equations can be solved by numeric computations. As can be observed from Fig. 2, a discontinuity arises where relative velocity attains zero value which leads to the halt of the integration process. To overcome this problem, Leine et al. [26] presented a switching method which has been used for this study.

Velocity-dependent friction force $f_{v_{\text{rel}}}$ is defined as

$$\text{for} |v_{\text{rel}}| \leqslant \eta \,(\text{Stick Phase}), \quad f(v_{\text{rel}}) = \min(|F_{f_s}|, \mu_s N)\,\text{sgn}(F_{f_s}); \tag{7}$$

$$\text{for} |v_{\text{rel}}| > \eta \,(\text{Slip Phase}), \quad f(v_{\text{rel}}) = \mu(v_{\text{rel}}) N\,\text{sgn}(v_{\text{rel}}). \tag{8}$$

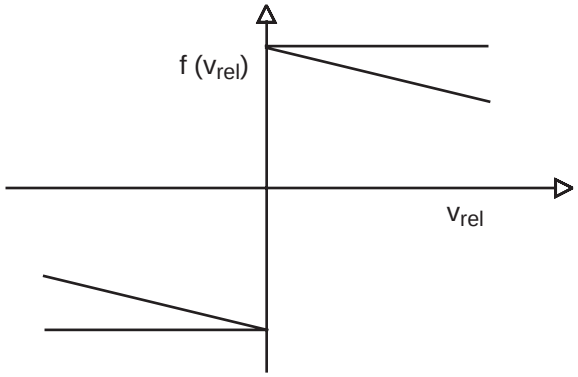

Fig. 2. The dependence of friction force on relative velocity.

Table 1
Summary of the cases considered for the parametric studies

Case no.	Base parameters (for rotor and pad)	Friction characteristics
Case I-A	Different mass, same damping; $m_1 = 0.5$, $m_2 = k_1 = k_2 = 1$, $c_1 = c_2 = 0.01$, $\mu_s = 0.6$, $\mu_k = 0.4$	Fixed friction characteristics
Case I-B	Same mass, different damping; $m_1 = m_2 = k_1 = k_2 = 1$, $c_1 = 0.56$, $c_2 = 0.01$	Fixed friction characteristics
Case II-A	Different mass, same damping; $m_1 = 0.5$, $m_2 = k_1 = k_2 = 1$, $c_1 = c_2 = 0.01$	Nonlinear variation in friction force $\alpha = 0.012$
Case II-B	Same mass, different damping; $m_1 = m_2 = k_1 = k_2 = 1$, $c_1 = 0.16$, $c_2 = 0.01$	Nonlinear variation in friction force $\alpha = 0.012$
Case II-C	Same mass, different damping; $m_1 = m_2 = k_1 = k_2 = 1$, $c_1 = 0.56$, $c_2 = 0.01$	Nonlinear variation in friction force $\alpha = 0.012$

3. Parametric studies

This section presents parametric studies for the cases summarized in Table 1. Coupling stiffness (k_3) is varied and phase state plots are used to illustrate limit cycles of rotor and pad.

In all the cases considered, the value of normal force (N) is taken as 10 and imposed velocity of the disc (v) as 1. The values for m_1, m_2, k_1, k_2, c_1, c_2, N, v and α are chosen to be in line with Shin et al. [24] to have a basis for a comparison of the results.

4. Results

4.1. Fixed friction characteristics

4.1.1. Case I-A

Friction coefficients (static and kinetic) were considered as constants, viz., $\mu_s = 0.6$ and $\mu_k = 0.4$, respectively. The phase space diagram for $m_1 = 0.5$, $m_2 = k_1 = k_2 = 1$ and $c_1 = c_2 = 0.01$ is given in Fig. 3(a). x_1 and x_1d are the displacement and velocity of the pad, respectively.

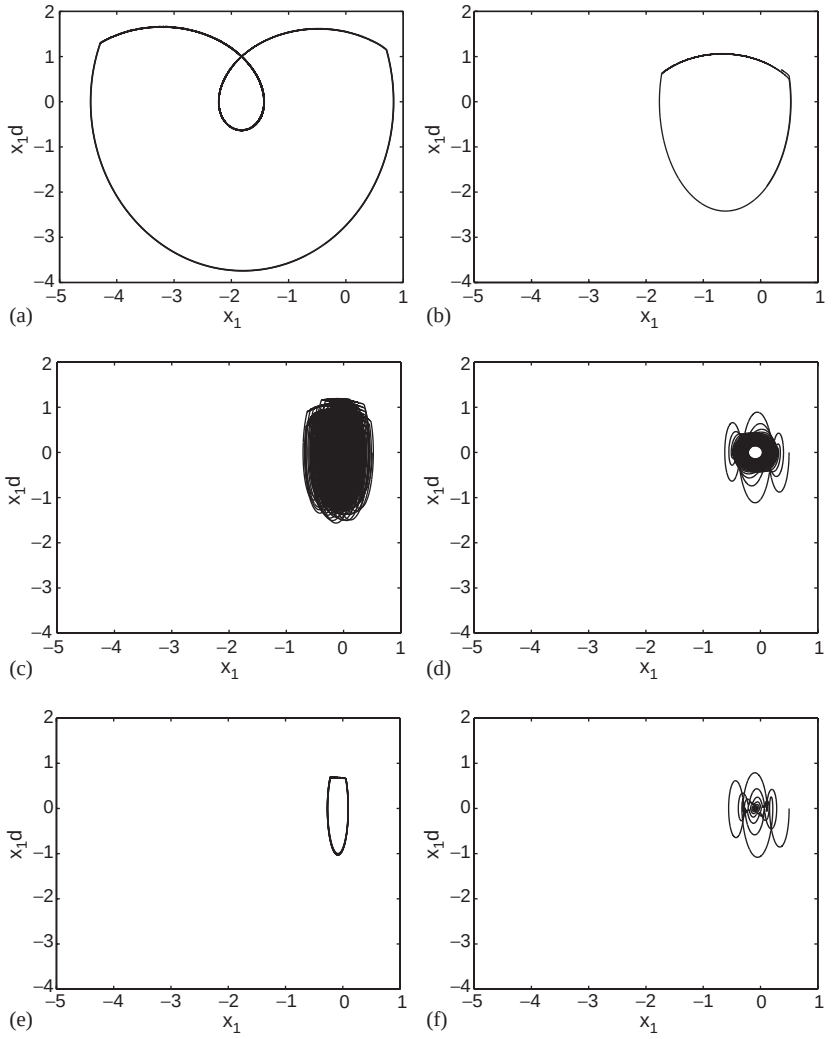

Fig. 3. Fixed friction characteristics $\mu_s = 0.6$ and $\mu_k = 0.4$; $m_1 = 0.5$, $m_2 = k_1 = k_2 = 1$. (a) Limit cycle motion of the pad $c_1 = c_2 = 0.01$, $k_3 = 0$, $c_3 = 0$. (b) Limit cycle motion of the pad $c_1 = c_2 = c_3 = 0.01$, $k_3 = 1$. (c) Motion of the pad $c_1 = c_2 = c_3 = 0.01$, $k_3 = 10$. (d) Motion of the pad $c_1 = c_2 = 0.01$, $c_3 = 0.1$, $k_3 = 10$. (e) Limit cycle motion of the pad $c_1 = 0.1$, $c_2 = 0.01$, $c_3 = 0.01$, $k_3 = 10$. (f) Motion of the pad $c_1 = 0.2$, $c_2 = 0.01$, $c_3 = 0.01$, $k_3 = 10$.

Introduction of the coupling stiffness ($k_3 = 1$) into the system reduced the size of the limit cycle (Fig. 3(b)). With higher values of k_3, the system starts to become unstable and at $k_3 = 10$, the system becomes unstable as is apparent from Fig. 3(c). Addition in damping at contact ($c_3 = 0.1$), however, makes the system stable (Fig. 3(d)). Adding the same amount of damping in the pad ($c_1 = 0.1$) instead of at the contact helps to limit the size of the limit cycle (Fig. 3(e)). Further increase in damping at pad ($c_1 = 0.2$) leads to a stable system (Fig. 3(f)).

4.1.2. Case I-B

Test runs were conducted using the following parameters: $m_1 = m_2 = k_1 = k_2 = 1$; $c_1 = 0.56$, $c_2 = 0.01$. Constant coefficients of friction were used ($\mu_s = 0.6$ and $\mu_k = 0.4$). The signature changes as the coupling stiffness is increased from $k_3 = 4$ (Fig. 4(c)) to $k_3 = 5$ (Fig. 4(d)).

4.2. Nonlinear variation in friction force

4.2.1. Case II-A

The nonlinear variation in friction force was taken into account with $\alpha = 0.012$. A negative gradient was considered for the runs. Different values for mass were taken, with damping values as low as 0.01. The system was observed at the coupling stiffness values of 1, 10 and 30 with $m_1 = 0.5$, $m_2 = k_1 = k_2 = 1$, $k_3 = 1$ and $c_1 = c_2 = c_3 = 0.01$. Shin et al. [24] have also *considered*

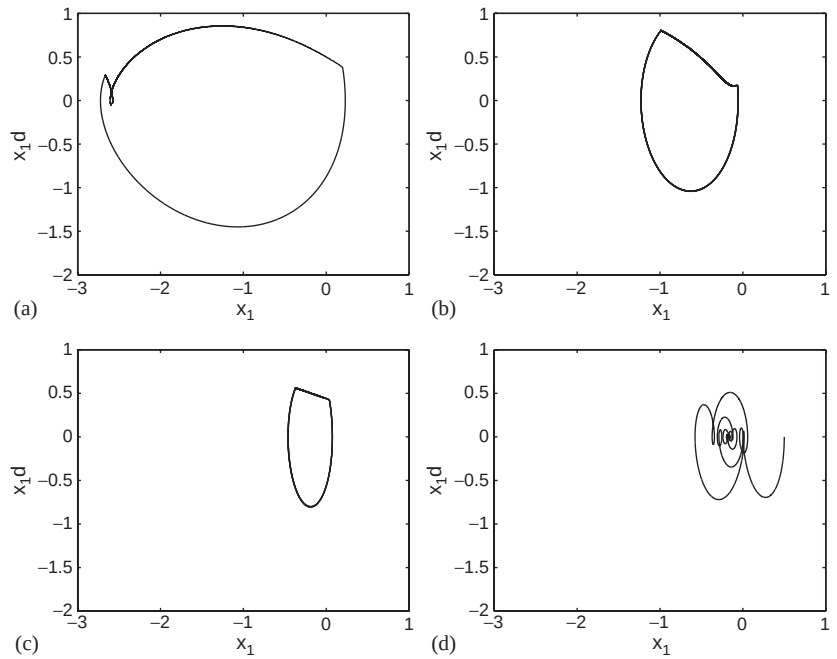

Fig. 4. Fixed friction characteristics $\mu_s = 0.6$ and $\mu_k = 0.4$; $m_1 = m_2 = k_1 = k_2 = 1$, $c_1 = 0.56$, $c_2 = 0.01$. (a) Limit cycle motion of the pad, $k_3 = 0$, $c_3 = 0$. (b) Limit cycle motion of the pad $k_3 = 1$, $c_3 = 0$. (c) Limit cycle motion of the pad $k_3 = 4$, $c_3 = 0$. (d) Motion of the pad $k_3 = 5$, $c_3 = 0$.

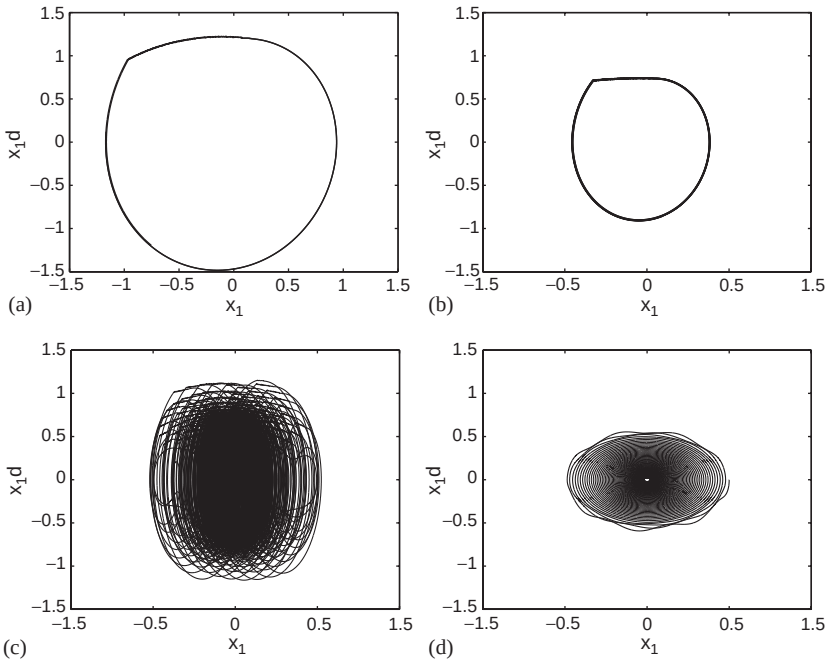

Fig. 5. Nonlinear friction characteristics $\alpha = 0.012$; $m_1 = 0.5$, $m_2 = k_1 = k_2 = 1$. (a) Limit cycle motion of the pad $c_1 = c_2 = 0.01$, $k_3 = 0$, $c_3 = 0$. (b) Limit cycle motion of the pad $c_1 = c_2 = 0.01$, $k_3 = 1$, $c_3 = 0.01$. (c) Motion of the pad $c_1 = c_2 = c_3 = 0.01$, $k_3 = 10$. (d) Motion of the pad $c_1 = c_2 = 0.01$, $c_3 = 0.2$, $k_3 = 30$.

this case without considering coupling stiffness. The results can be compared as follows. It was observed that with the increase in coupling stiffness, defined by the stiffness of the friction layer, the limit cycle reduces (Figs. 5(a) and (b)) and then the instability in the pad increases (Fig. 5(c)). However with the inclusion of damping, $c_3 = 0.2$, the system becomes stable (Fig. 5(d)).

4.2.2. Case II-B

In this case, the friction force–velocity gradient is $\alpha = 0.012$, $m_1 = m_2 = k_1 = k_2 = 1$, $c_1 = 0.16$ and $c_2 = c_3 = 0.01$. The limit cycle with $k_3 = 0$ is shown in Fig. 6(a), which is same as shown by Shin et al. [24]. The limit cycle reduces with increase in coupling stiffness as is apparent from a comparison of Figs. 6(a)–(d). It is apparent from the comparison of Figs. 6(e) and (f), that increase in damping at the contact $c_3 = 0.1$ is more effective in damping the motion instead of an increase at the disc, $c_2 = 0.1$.

4.2.3. Case II-C

In this case with nonlinear friction characteristics $\alpha = 0.012$ other parameters are $m_1 = m_2 = k_1 = k_2 = 1$; $c_1 = 0.56$ and $c_2 = 0.01$. Fig. 7(a) is obtained with $k_3 = c_3 = 0$. The results tally with the work from Shin et al. [24]. An increase in coupling stiffness $k_3 = 1$ immediately reduced the limit cycle to zero (Fig. 7(b)).

The summary of the results is presented in Tables 2 and 3.

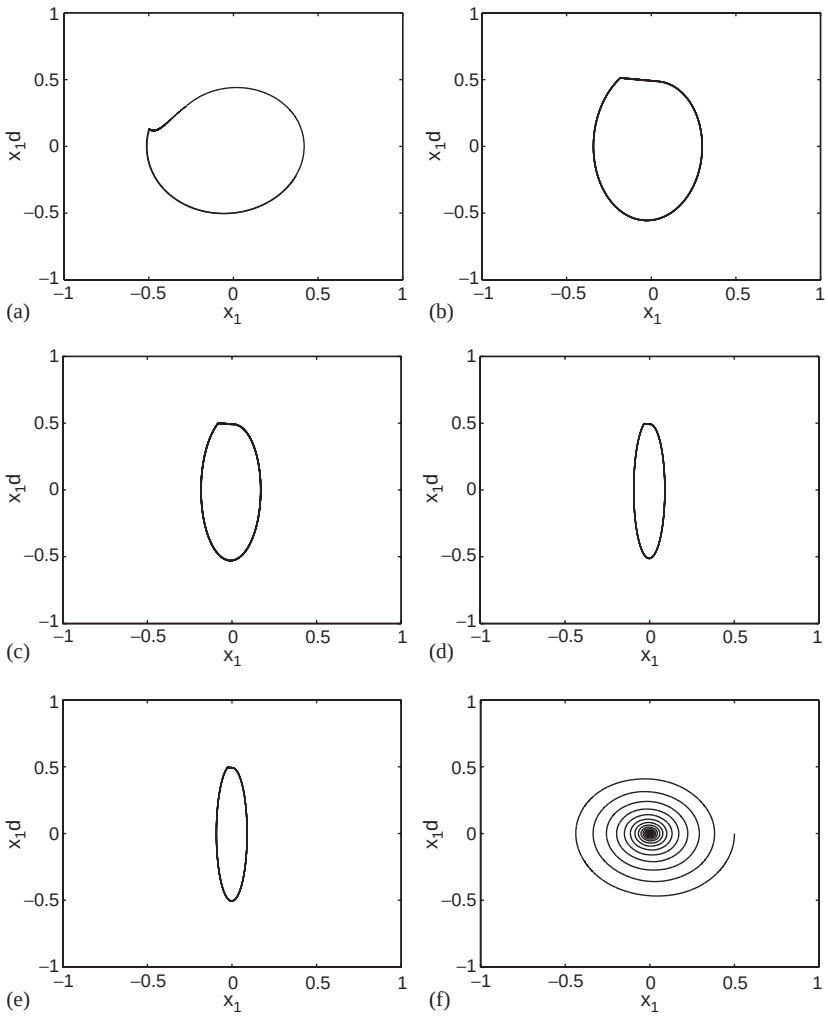

Fig. 6. Nonlinear friction characteristics $\alpha = 0.012$; $m_1 = m_2 = k_1 = k_2 = 1$; $c_1 = 0.16$. (a) Limit cycle motion of the pad, $k_3 = 0$, $c_2 = 0.01$, $c_3 = 0.01$. (b) Limit cycle motion of the pad, $k_3 = 1$, $c_2 = 0.01$, $c_3 = 0.01$. (c) Limit cycle motion of the pad $k_3 = 4$, $c_2 = 0.01$, $c_3 = 0.01$. (d) Limit cycle motion of the pad $k_3 = 15$, $c_2 = 0.01$, $c_3 = 0.01$. (e) Limit cycle motion of the pad $k_3 = 15$, $c_2 = 0.1$, $c_3 = 0.01$. (f) Limit cycle motion of the pad $k_3 = 15$, $c_2 = 0.01$, $c_3 = 0.1$.

5. Conclusions

The coupling stiffness between rotor and pad varies due to the growth of friction layers on the contact surfaces of rotor and pad. Using numerical modeling and computation, the effect of the variation of coupling stiffness on system stability has been studied. A 2-DOF model has been analyzed and discussed. The parametric values were chosen the same as by Shin et al., for the purpose of comparison. Phase space plots were used to illustrate the limit cycle motion of rotor and pad for different sets of mass, stiffness and damping. A larger size of the limit cycle represents

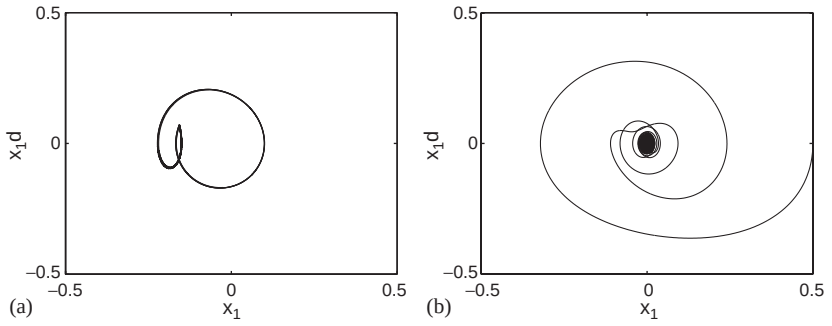

Fig. 7. Nonlinear friction characteristics $\alpha = 0.012$; $m_1 = m_2 = k_1 = k_2 = 1$; $c_1 = 0.56$; $c_2 = 0.01$. (a) Limit cycle motion of the pad $k_3 = 0$, $c_3 = 0$. (b) Motion of the pad $k_3 = 1$, $c_3 = 0$.

Table 2
Summary of the parametric studies for $\mu_s = 0.6$ and $\mu_k = 0.4$

Case no.	Friction characteristics	Comments
Case I-A	Fixed friction characteristics. $\mu_s = 0.6$, $\mu_k = 0.4$. Different mass, same damping; $m_1 = 0.5$, $m_2 = k_1 = k_2 = 1, c_1 = c_2 = 0.01$	System becomes unstable with increase in coupling stiffness. Addition of damping reduced the size of limit cycle. It was found that addition of damping at the contact reduced the limit cycle to zero and stabilized the system faster than adding damping at the pad or rotor disc
Case I-B	Fixed friction characteristics. Same mass, different damping; $m_1 = m_2 = k_1 = k_2 = 1$, $c_1 = 0.56$, $c_2 = 0.01$	Increase in stiffness reduced the limit cycle to zero. Change in system motion pattern was also observed with increase in stiffness

Table 3
Summary of the parametric studies for $\alpha = 0.012$

Case no.	Friction characteristics	Comments
Case II-A	$\alpha = 0.012$. Different mass, same damping; $m_1 = 0.5$, $c_1 = c_2 = 0.01 m_2 = k_1 = k_2 = 1$	System became unstable with increase in coupling stiffness. Addition of damping stabilized the system
Case II-B	$m_1 = m_2 = k_1 = k_2 = 1$, $c_1 = 0.16$, $c_2 = 0.01$, $\alpha = 0.012$	Increase in stiffness reduced the limit cycle size. Limit cycle continued to decrease while velocities attained high values
Case II-C	$\alpha = 0.012$. Same mass, different damping; $m_1 = m_2 = k_1 = k_2 = 1$; $c_1 = 0.56$, $c_2 = 0.01$	A small increase in coupling stiffness reduced the limit cycle to zero

the noisier state of the system. In a case with non-unity mass ratio and negligible damping, the size of the limit cycle increased with a small increase in the coupling stiffness irrespective of friction characteristics. When the mass ratio was unity and friction coefficients were constants, the system motion pattern changed significantly with a slight change in coupling stiffness. Systems with high damping values and nonlinear friction characteristics stabilized quickly with a slight increase in coupling stiffness. It was found that system behavior is affected by the combination of parameters, such as damping, mass ratios and coupling stiffness. In the study, it is shown that the stiffness of the friction layer also plays a role in the system's behavior, as variation in its value may stabilize or destabilize the system. Hence its influence should be taken into account while studying the stick–slip motion of the brake system.

This paper presented an analytical model, which demonstrated the significance of the stiffness of the friction layer. Since different friction layers develop at different braking conditions, the stiffness continues to change with time, with change in contact pressure, temperature and environment conditions [3]. Hence, each brake pad-rotor assembly should be studied independently. As part of future studies, dynamometer tests as well as field tests will be conducted and the stiffness of the friction layer will be measured using nanoindentation. These realistic values will then be used in the extended Shin et al. method proposed in this paper, to investigate noise and vibration.

References

[1] G.D. Liles, Analysis of disc brake squeal using finite element methods, SAE 891150.
[2] D. Inman, *Engineering Vibrations*, second ed, Prentice-Hall, Englewood Cliffs, NJ, 2001.
[3] P. Filip, Friction and wear of polymer matrix composite materials for automotive braking industry, in: *Braking 2002, IMechE, International Conference of Automobile Braking*, Leeds, UK, 2002, pp. 341–354.
[4] P. Filip, L. Kovarik, M. Wright, Automotive brake lining characterization, SAE 97B-2.
[5] N. Millner, An analysis of brake squeal, SAE 780332.
[6] K.B. Dunlop, M.A. Riehle, R.E. Longhouse, Investigative overview of automotive disc brake noise, SAE 1999-01-0142.
[7] W. Liu, J. Pfeifer, Reducing high frequency disc brake squeal by pad shape optimization, SAE 2001-01-0447.
[8] P. Filip, Z. Weiss, D. Rafaja, On friction layer formation in polymer matrix composite materials for brake applications, *Wear* 252 (2001) 189–198.
[9] L. Gudmad-Hoyer, Tribological properties of automotive disc brakes with solid lubricants, *Wear* 232 (1999) 165–175.
[10] R. Holinski, Fundamentals of dry friction and some practical examples, *Industrial Lubrication and Tribology* 53 (2) (2001) 61–65.
[11] P. Lamarque, Brake squeal, the experiences of manufacturers and operators, Progress Report 8500 B, Institute of Automobile Engineers, Research and Standardization Committee, 1934.
[12] D. Sinclair, Frictional vibrations, *Journal of Applied Mechanics* (1955) 207–214.
[13] R. Spurr, A theory of brake squeal, in: *Proceedings of the Automotive Division*, vol. 1, IMechE, 1961, pp. 33–40.
[14] S. Earles, C.K. Lee, Instabilities arising from the friction interaction of a pindisc system resulting in noise generation, *Journal of Engineering for Industry* 98 (1) (1976) 81–86.
[15] M. North, A mechanism of disc brake squeal, in: *14th FISITA Congress*, no. 9 in 1, 1972.
[16] J. Flint, Modeling of high frequency disc brake squeal, in: *Braking 2000, IMechE, International Conference of Automobile Braking*, Leeds, UK, 2000, pp. 39–50.
[17] J. Fieldhouse, C. Beveridge, A comparison of disc and drum brake rotor mode movement, in: *Seoul 2000, FISITA World Congress*, F2000H241, 2000.

[18] Y. Sasaki, Development of non-asbestos friction materials, ara- mid fibers, in: *Proceedings of 5th Akzo Symposium*, 1988, pp. 1–12.
[19] P. Ioannidis, P.C. Brooks, D.C. Barton, M. Nishiwaki, Brake system noise and vibration—a review, in: *Braking 2002, IMechE, International Conference of Automobile Braking*, Leeds, UK, 2002, pp. 53–73.
[20] A. Anderson (Ed.), *Friction Lubrication and Wear Technology*, first ed., ASME Handbook, vol. 18, ASME International, New York, 1992, pp. 569–609.
[21] C. Langlade, S. Fayeulle, R. Olier, New insights into adhesion and lubrication properties of graphite-based transfer films, *Wear* 172 (1994) 85–92.
[22] M. Jacko, R. DuCharme, New insights into adhesion and lubrication properties of graphite-based transfer films, SAE 730191.
[23] P. Blau, *Friction Science and Technology*, Marcel Dekker, New York, 1996.
[24] K. Shin, M. Brennan, J. Oh, C. Harris, Analysis of disc brake noise using a two-degree-of freedom model, *Journal of Sound and Vibration* 254 (5) (2002) 837–848.
[25] K. Tzou, J. Wickert, A. Akay, In-plane vibration modes of arbitrary thick discs, *Journal of Vibrations and Acoustics* 120 (2) (1998) 384–391.
[26] R. Leine, D. Campen, A. Kraker, L. Steen, Stick slip vibrations induced by alternate friction models, *Non Linear Dynamics* 16 (1998) 41–54.